V15

Characerization of silicon strip sensors

with the Educational Alibava System

Developed by
Nora Held and Falko Barth
edited by
Felix Wizemann
translated by
Hannah Jansen

Contents

technische universität
dortmund

1 Introduction

1.1 Aim of the experiment

The aim of this experiment is to make the functioning of a silicon semiconductor detector understandable and to examine its properties in several experimental tasks. In addition to the sensor, the readout electronics and data processing are also considered. The data obtained and their processing should give an impression of how the detection of particle tracks in large experiments such as the ATLAS detector at the LHC[1] proceeds.

1.2 Preliminary note

The system used, from the company Alibava Systems[2], is called **E**ducational **A**libava **Sy**stem (**EASy**). It has been specially developed for students due to its simplicity in handling the apparatus and the software for data acquisition. This system allows measurement tasks to be carried out easily and safely.
The subject of this experiment is both an exact characterisation of the strip sensor and the measurement with a strontium-90 source. This emits radioactive radiation in the form of β^-−radiation. It is sufficiently shielded by the experimental setup.

2 The ATLAS detector

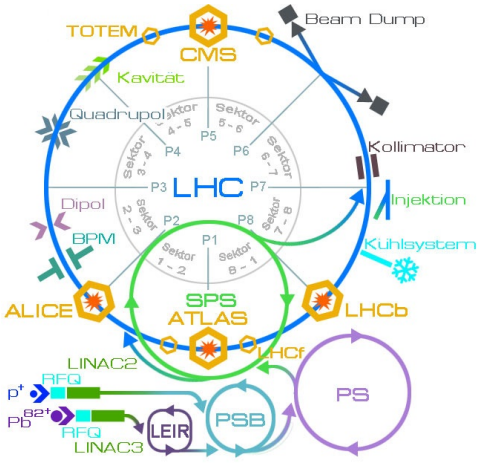

Fig. 2.1: Experiments of the LHC (CERN).

The CERN nuclear research centre in Geneva has set itself the task of researching the structure of matter. The LHC has a circumference of just under 27 km. There are a total of four large experiments at it: ALICE, LHCb, CMS and ATLAS, in which protons are made to collide. Figure 2.1 shows this and other components. Figure 2.3 shows a schematic representation of the ATLAS detector.
The ATLAS detector is built cylindrically around the beam tube in which the particles collide. It is constructed in several layers. Directly at the beam tube is the so-called *Inner Detector* (ID), which currently (2018) consists of the *Pixel Detector*, the *Silicon Strip Detector* (SCT[3]) and the

[1] LHC = **L**arge **H**adron **C**ollider
[2] A result of a long-term collaboration between the IMB-CNM in Barcelona, the IFIC in Valencia and the University of Liverpool
[3] Semiconductor Tracker

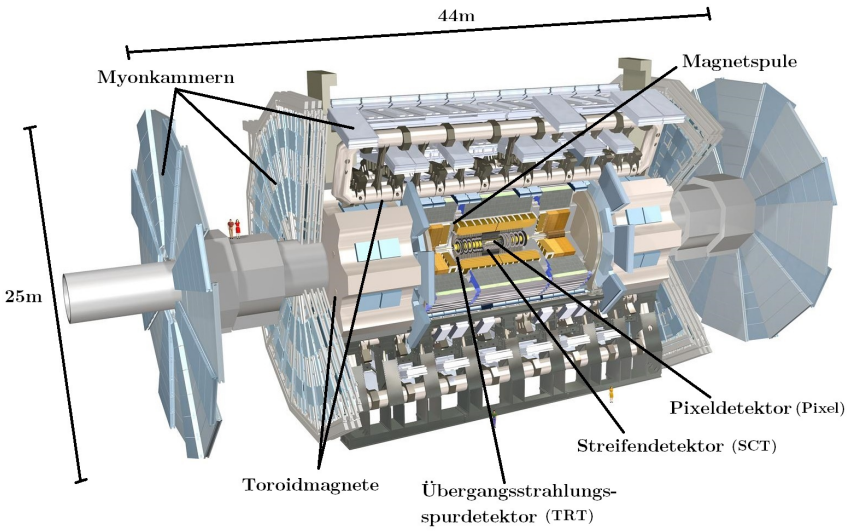

Fig. 2.3: Schematic drawing of the ATLAS detector. ([Peq08], edited)

Transition Radiation Tracker (TRT).

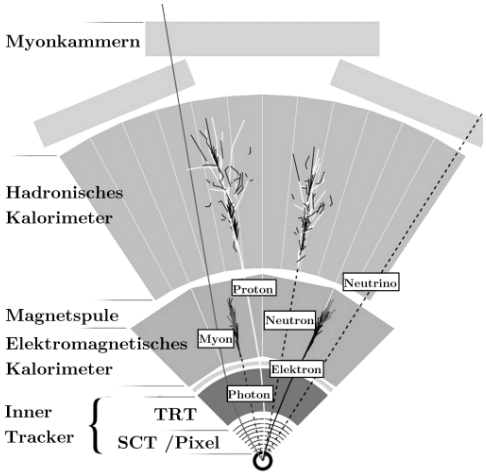

Fig. 2.2: Cross-section of the ATLAS experiment and schematic representation of the particle tracks. ([PS13], edited)

Pixel sensors differ from strip detectors in that they are more highly structured and thus have a higher spatial resolution. However, because pixel sensors are more expensive to produce, they are only used in the innermost layers of the ID.

The ID is surrounded by a magnetic coil. Charged particles are thus deflected onto curved paths by the Lorentz force. The momentum and charge of the particles are calculated from the path, which can be calculated from the measurement results of the ID. Figure 2.2 shows the course of some particle tracks in ATLAS.

The second innermost layer of the ATLAS detector is the silicon strip detector. It is directly connected to the pixel detector and consists of four double layers of silicon strip sensors that are twisted by 40 mrad. This improves the resolution along the strips.

In total, the SCT consists of 4088 individual modules, each of which contains 768 strips. The apparatus from the company Alibava Systems examined in the experiment contains a sensor that has 128 individual strips [Ali15]. Handling its amount of data gives an idea of the dimension of the data processed in the ATLAS experiment.

3 Semiconductor

3.1 General information about semiconductors

A semiconductor is a material whose properties lie between those of a *conductor* and those of an *insulator*. They have resistances between $10^{-6}\,\Omega$m and $10^{13}\,\Omega$m [Kit02]. Three groups can be distinguished: the *element semiconductors* such as germanium, silicon and selenium, the *compound semiconductors* such as gallium arsenide and the *organic semiconductors*, which consist of carbon compounds [Kuc11].

The electrical behaviour of semiconductors is characterised by the size of their band gap[4], which is defined as the energy gap E_g between the conduction and valence band (cf. figure 3.1). In a conductor, the bands overlap so that there are enough charge carriers in the conduction band. One speaks of an insulator from a band gap of 4 eV. Here, the energy to be expended is too great for electrons to leave the valence band. A semiconductor has neither such a large band gap as an insulator, nor do the bands overlap as in a conductor [Kit02].

The subject of this investigation is a silicon crystal. Silicon is a typical elemental semiconductor with four electrons in the valence band and a band gap of 1.107 eV [Kuc11]. The atoms arrange themselves in a diamond lattice structure [Kit02] where they each have four nearest neighbours. Each of the four valence electrons contributes to the bonding of the four neighbours.

Fig. 3.1: Band diagram of an elemental semiconductor such as silicon. Electrons are excited into the conduction band by supplying energy $\geq E_g$ (according to [Kit02]).

At a temperature of 0 K, the element semiconductor has no electrical conductivity. Due to thermal excitations, electrons can leave the covalent bonds and jump into the conduction band. They leave behind the positively charged atomic body. This resulting "hole" can be regarded as a quasiparticle with an effective mass. The electron is bound to the Coulomb field of the atomic body without external force, so recombination occurs again. However, if an electric field is applied, the electrons move to the anode while the holes move in the opposite direction.

This process is referred to as intrinsic conduction. Silicon as an intrinsic semiconductor has a charge carrier density of $1.5 \cdot 10^{10}\,\mathrm{cm}^{-3}$. In order to increase the conductivity of a semiconductor crystal, the band gap can be reduced by deliberately introducing foreign atoms. This process is called *doping*[5]. The introduction of the impurities increases the

[4]For more information see Kittel, chapter Band model.
[5]lat. dotare = to equip

charge carrier density, which leads to an improvement in conductivity.

3.2 p- and n-type semiconductors

Since silicon has four electrons in the valence band, suitable impurities are those that have either three or five valence electrons [Kit02]. Depending on the type of doping, a distinction is made between a p-type and an n-type semiconductor.

n-type semiconductor

In this type of doping, a lattice atom of the silicon crystal is exchanged for a foreign atom that has one electron more in the valence band than silicon. Figure 3.2 shows this schematically in two dimensions. Doping with arsenic was chosen as an example here. As an element of the fifth main group, arsenic has five electrons in the valence shell, so that one of the electrons is superfluous for the bond in the lattice. This electron could move freely in the lattice if it were not bound to the Coulomb field of the atomic body. Arsenic that is doped in silicon is therefore referred to as a *donator*[6].

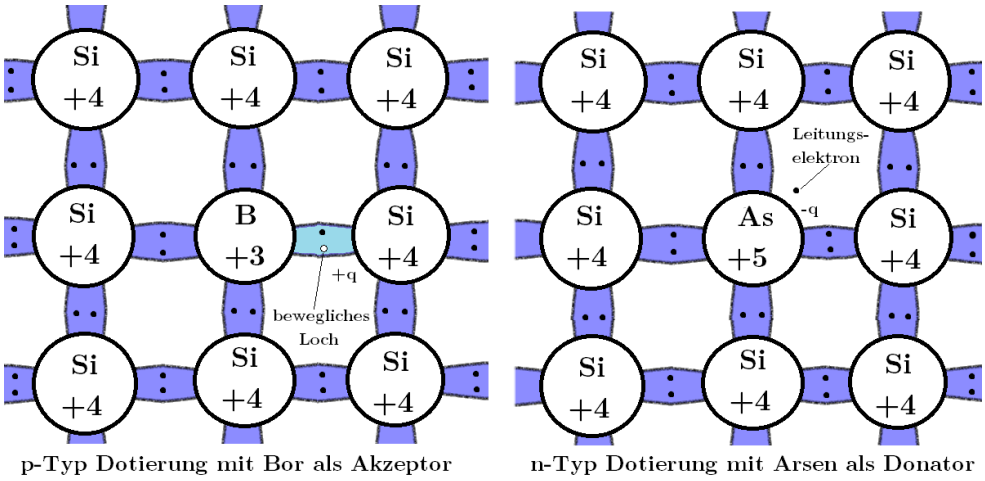

Fig. 3.2: Schematic representation of an n- and p-type doping in two dimensions (similar [SL13]).

p-type semiconductor

In a p-type semiconductor, the silicon crystal is doped with an element that has fewer than four electrons in the valence shell. Figure 3.2 shows this for the example of boron. The boron atom replaces a silicon atom in the crystal lattice. Since it is an element of the third main group, only the three electrons in the valence shell are involved in the bond to the four neighbouring atoms.

[6]lat. donare = to give

The compound is electrically neutral, but the lattice structure lacks a binding electron in one of the covalent bonds. The hole created here can be filled by electron capture, which is why such a foreign atom in a silicon crystal is also called an acceptor[7]. Thus, the hole can be regarded as a free charge carrier with a positive charge.
In both cases, the current flow is determined by diffusion and drift velocity of the charge carriers. Holes and electrons can be treated physically the same and the holes can be considered as positively charged charge carriers.

3.3 The pn transition

In semiconductor technology, one of the simplest components is the diode. In the diode, a p-doped semiconductor layer is connected to an n-doped one, which is called a *pn transition*. In the following, the terms p- and n-side are used for short. The property of the pn transition of a simple diode is also elementary for semiconductor particle detectors such as the pixel and stripe detector of the ATLAS experiment.
The pn transition initially causes charge carrier diffusion between the layers, since the n-side has an excess of electrons and the p-side has an excess of holes. The electrons of the n-side recombine with the holes of the p-side. Due to the stationary atomic hulls, the n-side becomes slightly positively charged and the p-side slightly negatively charged. A dynamic equilibrium between diffusion and opposite electrical drift is established. The potential difference in this equilibrium is material dependent and is denoted by U_D for diffusion voltage[8]. U_D is of the order of a few mV [Har09].
For the detection of particles, a positive potential is applied to the n-side and a negative potential to the p-side. The electrons of the negatively charged cathode recombine with the holes of the p-side and the conduction electrons of the n-side drift to the positively charged anode. Thus, a depletion of charge carriers occurs at the pn junction, since all free charge carriers have been removed by the external field. This zone is called *barrier layer* or also *depletion zone*. Its thickness $d(U)$ depends on the applied bias voltage U as follows:

$$d(U) = \sqrt{\frac{2\varepsilon(U_D + U)}{qN_{\text{eff}}}} \quad , \tag{1}$$

where ε is the dielectric constant of silicon, U_D is the described diffusion voltage in dynamic equilibrium, q is the elementary charge and N_{eff} is the effective charge carrier density of the crystal described by formula (2). N_D and N_A are the respective doping concentrations

[7] lat. acceptare = to accept
[8] More correct, but rarely used, is the term *anti-diffusion voltage*, since U_D counteracts the difussion of the charge carriers

of donors and acceptors.

$$N_{\text{eff}} = \frac{N_D N_A}{N_D + N_A} \tag{2}$$

If the depletion zone is spread over the entire crystal, one speaks of full depletion and the necessary *depletion voltage* U_{dep}.
Typically, there is $U \gg U_D$, so that the diffusion voltage can be neglected. From this, the estimation is obtained by rearranging formula (1):

$$d(U) = \sqrt{\frac{2\varepsilon U}{qN_{\text{eff}}}} \quad . \tag{3}$$

And since the thickness of the depletion zone reaches its maximum at U_{dep}, it follows after rearranging formula (3)

$$U_{dep} \approx \frac{q}{2\varepsilon} N_{\text{eff}} D^2 \tag{4}$$

with the sensor thickness D. If the applied voltage U is below the depletion voltage U_{dep}, only a fraction of the material is depleting. The thickness d_c of the depletion zone can be approximated with:

$$\begin{aligned} d_c(U) &= D\sqrt{\frac{U}{U_{dep}}} && \text{für } U < U_{dep} \\ d_c(U) &= D && \text{für } U \geq U_{dep} \quad . \end{aligned} \tag{5}$$

The energy deposition of an ionising particle can only be detected to its full extent when the sensor is fully depleting and thus generated electron-hole pairs do not recombine directly. Ideally, no current flows through the semiconductor in this situation, as it has no free charge carriers. In reality, however, thermal excitation leads to the formation of unwanted electron-hole pairs, which are then prevented from recombining by the applied bias voltage in the depletion zone and are conducted to the poles, which is referred to as *leakage current*. Since the potential at the poles increases with increasing voltage and thus more energy is supplied to the crystal, the leakage current increases with the applied bias voltage. If the leakage current is measured as a function of the applied voltage, a curve as shown in figure 3.3 typically results. This measurement can be used to estimate at which voltage the crystal is fully depleting, since the leakage current initially increases strongly with the applied bias voltage and after reaching the depletion voltage only increases linearly up to the breakdown voltage.

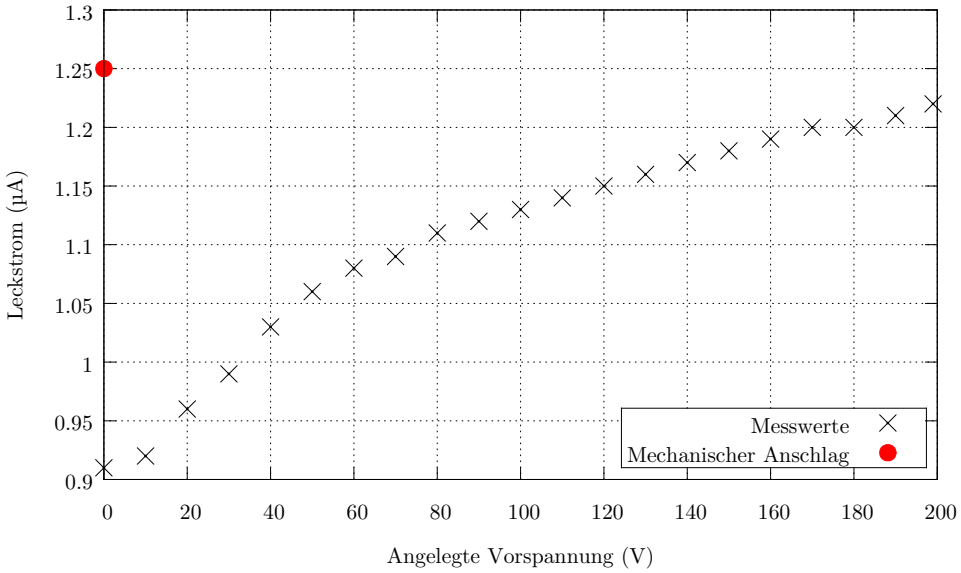

Fig. 3.3: Current-voltage characteristic curve of the Educational Alibava system. The depletion voltage U_{dep} can be estimated from the flattening of the curve at 60 V. Note that the adjustment knob for the bias voltage is not turned to the mechanical stop, as here the voltage is applied minimally in the forward direction, which leads to the value marked in red.

4 Interaction with ionising radiation

The EASy makes it possible to detect ionising particles and record their charge deposition. The following theoretical aspects help to analyse and interpret the spectrum.

4.1 The beta decay

Ionising particles produced in radioactive decays are, for example, α and β particles, as well as γ radiation and result from the decay of an unstable atomic nucleus. The decay rate and the associated emission of particles is determined by the activity and the half-life. The activity is defined in equation 6 and has the dimension Bq=$[\frac{1}{s}]$ [Bet96]:

$$A = \lambda N = -\frac{\mathrm{d}N}{\mathrm{d}t} = \lambda N_0 \mathrm{e}^{-\lambda t} = A_0 \mathrm{e}^{-\lambda t}\,. \tag{6}$$

N_0 indicates the number of nuclei at the start of observation of the decay. λ is the so-called decay constant of the primary decay.
The ^{90}Sr source to be used belongs to the pure β radiators [Leo87], in which a neutron is converted into a proton [Bet96].

$$\mathrm{n} \rightarrow \mathrm{p} + \mathrm{e}^- + \bar{\nu} \tag{7}$$

A typical energy spectrum of a β emitter is shown in Figure 4.1. The spectrum arises

because the decay energy is divided between the electron, the antineutrino and the atomic nucleus.

The emitted β^- particles of the ^{90}Sr source are electrons with a maximum kinetic energy of 0.546 MeV [Leo87]. The decay chain of ^{90}Sr is as follows [Rau]:

$$^{90}\mathrm{Sr} \xrightarrow{\beta^-} {}^{90}\mathrm{Y} \xrightarrow{\beta^-} {}^{90}\mathrm{Zr}\,. \tag{8}$$

The decay of yttrium into zirconium is also an almost pure β^- decay with an emission energy of 2.28 MeV.

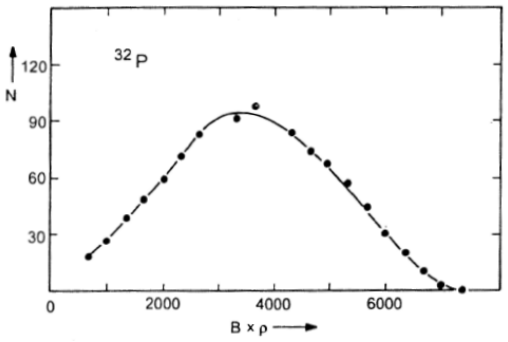

Fig. 4.1: „Electron spectrum of a β decay measured with a magnetic spectrometer “ [Bet96].

4.2 Interaction of electrons with matter

Unless electrons with a kinetic energy $E_{\mathrm{kin}} > 0$ are in a vacuum, interactions occur with the matter that surrounds them. The interactions that occur are mainly the elastic collision with the nucleus and collisions with electrons of the atomic shell. [Leo87]

Because the kinetic energy of the emitted electrons of the ^{90}Sr source is not large enough, the bremsstrahlung, the inelastic collision with the atomic nuclei and the Cherenkov radiation are not considered in detail.

The detection of electrons crossing the silicon sensor is done via the ionisation of the atoms in the crystal lattice by collisions with shell electrons. The energy that the electron loses on average per distance is determined for electrons by the modified Bethe-Bloch equation [Leo87]:

$$-\frac{\mathrm{d}E}{\mathrm{d}x} = 2\pi \mathrm{N_a m_e c}\rho \frac{\mathrm{Z}}{\mathrm{A}} \frac{1}{\beta^2} \left[\ln\left(\frac{\tau^2(\tau+2)}{2(\mathrm{I}/\mathrm{m_e c^2})^2} \right) + \mathrm{F}(\tau) - \delta - 2\frac{\mathrm{C}}{\mathrm{Z}} \right] \tag{9}$$

Here τ has the unit $\mathrm{m_e c^2}$ and corresponds to the kinetic energy. For equation 9, $\mathrm{F}(\tau)$ and τ are determined as follows:

$$\mathrm{F}(\tau) = 1 - \beta^2 + \frac{\frac{\tau^2}{8} - (2\mathrm{r_e}+1)\ln 2}{(\tau+1)^2} \quad \text{mit} \quad \tau = \gamma - 1 \tag{10}$$

Table 4.1 gives an overview of all necessary constants and symbols.

From the modified Bethe-Bloch formula it follows that the average energy disposition of an ionising electron of the maximum energy of the primary decay of ^{90}Sr in pure silicon is 3.88 MeV/cm.

Table 4.1: Constants and formulae of the modified Bethe-Bloch equation.

Symbol	Meaning	Symbol	Meaning
r_e	Classic e^- Radius: $2{,}817 \cdot 10^{-13}$ cm	ρ	Density of the absorber material
m_e	Electron mass: $9{,}108 \cdot 10^{-28}$ g	β	$\frac{v}{c}$ of the incoming particle
N_a	Avogadro constant: $6{,}022 \cdot 10^{23}$ mol^{-1}	γ	$1/\sqrt{1-\beta^2}$
I	Average excitation potential: 173 eV	δ	Density correction
Z	Proton number	C	Envelope correction: -4,44
A	Nuclide number	$2\pi N_a m_e c$	0,1535 MeV cm^2/g

4.3 Energy spectrum in the silicon sensor

For silicon sensors, as a consequence of the central limit theorem, a Gaussian distribution can be expected as a spectrum of the deposited energy of traversing electrons at a sufficient thickness [Leo87].

However, in thinner sensors, such as the sensor in this experiment with a thickness of 300 μm, there are not enough interactions with the electrons of the atomic shells to apply the central limit theorem. Thus, the spectrum of the deposited energy cannot be sufficiently approximated by a Gaussian distribution.

In addition, not all secondary electrons are decelerated again in thin sensors and thus not all the energy emitted by the electron is absorbed. This ensures that the energy distribution becomes asymmetrical and resembles a Landau distribution [Ali15].

In thin silicon sensors, it should also be noted that the electrons of the β source are not monoenergetic. Therefore, the convolution of a Gaussian distribution with a Landau distribution describes the spectrum of the deposited energy most accurately [Sch14]. Such a spectrum is shown in figure 4.2. The MPV[9] is the most probable energy loss,

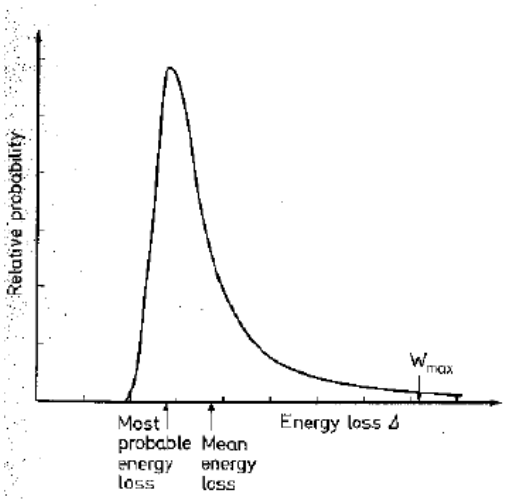

Fig. 4.2: Typical spectrum of an energy disposition of an electron in a thin sensor [Leo87].

[9]Most Probable Value

which in a Landau distribution is below the mean energy loss.
Note that the charge deposition is always given in ADC Charges or Counts[10]. The conversion of ADC charges into energies in units of keV is to be polynomially approximated and weighted with the energy to generate an electron-hole pair. The calibration of the system allows the conversion of ADC signals into generated electron-hole pairs. Together with the knowledge that 3.6 eV are needed to generate an electron-hole pair in silicon [Ali15], the deposited energy can now be determined.

[10]unit of output of the Analogue-to-Digital Converter(ADC)

5 Experimental setup

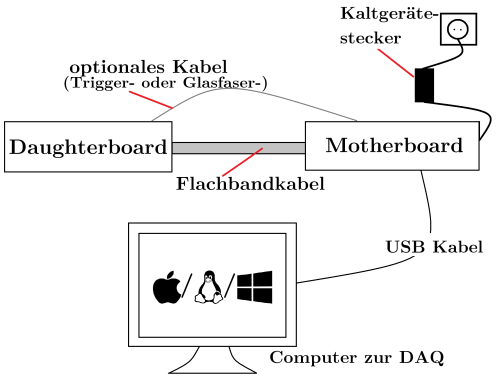

Fig. 5.1: Circuit diagram for setting up Alibava EASy. (Excerpts from iconarchive.com)

The Alibava EASy is a detector system consisting of three components: the control unit, the detector unit and a computer that controls the data acquisition. The software to control the system is done via the Alibava-gui[11].
The detector and control unit are first connected via a ribbon cable, which supplies the detector with voltage and transmits data to and command signals from the control unit. In addition, depending on the measurement, an optical fibre or a trigger cable may be necessary.
The control unit is then connected to the computer via a USB cable. Only then is the control unit to be supplied with power via the cold appliance plug and then the software to be started.

5.1 Detector unit

The detector unit contains the semiconductor sensor and the corresponding readout electronics. The silicon sensor is comparable to those of the ATLAS experiment and is divided into 128 strips. The readout chip used (BEETLE) is connected to the strips of the sensor via wirebonds. The BEETLE chip is used in the LHCb experiment.
Incoming charge signals are amplified in the BEETLE chip, converted into voltage signals and then held in a pipeline. With an incoming trigger, the control unit now queries the signal of the Alibava chip and receives the oldest element of the pipeline. If there is no trigger signal, the stored signals are discarded. In the control unit, the signal is now digitised and converted into so-called *ADC Counts*.
To measure efficiently, the sensor must be fully depleted. For the strip sensors used in the Alibava, the depletion voltage U_{dep} is typically in the range of $U_{dep} \approx 60$ to $80\,\mathrm{V}$ [Ali15]. The applied voltage can be adjusted on the control unit. Only operation in the blocking direction is possible.
On the top of the detector unit is a sliding platform that contains the laser system and a carbon plate. This has two different positions, which are designated in the following as (L) for the laser measurement and (Q) for the source measurement. In figure 5.2 the unit is shown in Q position.

[11] gui = graphical user interface

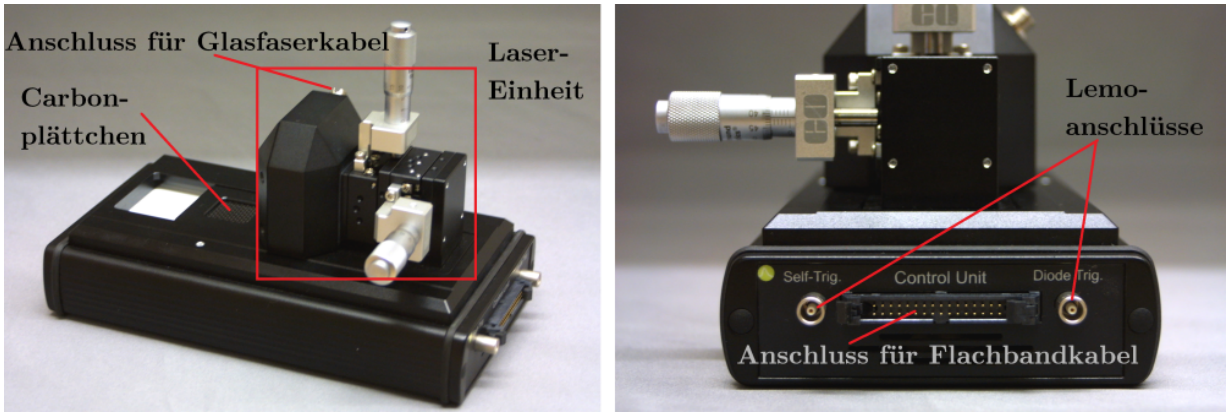

Fig. 5.2: Detector unit in top and front view.

The semiconductor sensor

The sensor built into Alibava EASy works according to the principle of a semiconductor detector explained in section 3.

The base consists of a 300 m thick, n-doped silicon layer, which is covered by a metallisation on the underside[12]. It is connected to a low ohmic resistor for power supply. There are 128 p-doped implants embedded in the n-doped base on the top. These are long and narrow, from which their name "strips" is derived. The strip sensors, in contrast to the base, are insulated from each other, which enables localisation of the deposited charge in the detector.

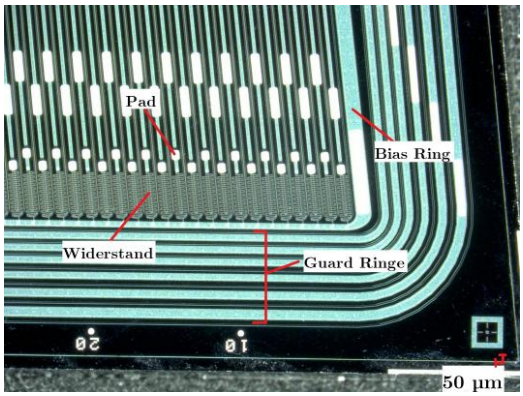

Fig. 5.3: Macroscopic image of a strip sensor (Photo: J. Lönker).

Furthermore, they are covered by a silicon oxide layer, which prevents the leakage current from flowing directly into the readout electronics. The p-doped implants are capacitively coupled with an aluminium electrode lying on the silicon oxide layer, which is read out via an ohmic contact. A macroscopic image of a stripe detector can be seen in figure 5.3 [Ali15].

The bias ring is used to supply the strips with voltage, while the guard rings ensure that the charge does not flow uncontrolled beyond the sensor into the electronics [CER16]. Figure 5.4 shows a schematic oblique image. Due to the p-implants read out in an n-base, such a sensor is called a p-in-n sensor.

If the sensor is not fully depleted, the electron-hole pairs recombine outside the depletion zone because they are not separated by the electric field. The charge collection efficiency,

[12]Note: Here the n^+ layer on the back of the sensor is neglected. This is important to maintain the function of the latter even when exposed to radiation. See [Har09] and [CER16] for this.

CCE[13], of the measurement increases with the thickness of the depletion zone until it reaches its maximum at U_{dep}.

For the built-in laser, the formula (5) gives the following relationship for the CCE of the detector:

$$\mathrm{CCE}(U) = \frac{1 - \exp(\frac{-d_c(U)}{a})}{1 - \exp(\frac{-D}{a})} \quad . \qquad (11)$$

with the thickness of the depletion zone d_c according to equation (5), a sensor thickness of $D = 300\,\mu$m and a mean penetration depth of laser into silicon a. This depends on the wavelength of the laser and has, for example, for 960 nm a value of 74 μm and for 1073 nm a value of 380 μm [Lid96]. For the detection of electrons, the CCE is proportional to the thickness of the depletion zone.

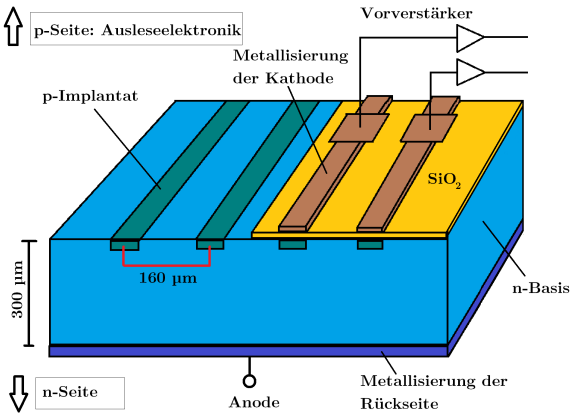

Fig. 5.4: Schematic diagram of the sensor installed in the EASy. The n-side is supplied with voltage via a connection, while the electrodes on the p-side can be read out individually (according to [Ali15]).

The Laser

The laser built into the system is used to measure and examine the built-in strip sensors. It is generated in the control unit and fed to the detector unit via a fibre optic cable. The platform must therefore be in the (L) position. The laser has a wavelength of 980 nm, a diameter of about 20 μm on the sensor and a peak power of 0.6 mW with a pulse length of 5 ns [Ali15].

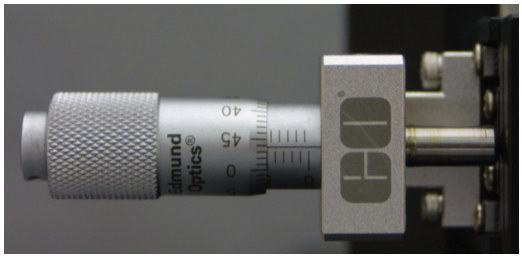

Fig. 5.5: Horizontal micrometer screw for positioning the laser above the sensor.

There are two micrometer screws on the laser unit that can be adjusted with an accuracy of 10 μm. With the vertical micrometer screw, the focus can be adjusted by the height of the laser. The horizontal micrometer screw is used to position the laser over the strip.

[13] Charge Collection Efficiency

5.2 Control unit

The control unit shown in figure 5.6 is used to control the detector unit. The bias voltage of the sensor can be adjusted via the rotary knob "Diode Bias". The flowing leakage current is registered via an amperemeter of the control unit and can be read in 0.01 μm steps.

Fig. 5.6: Control unit of EASy.

Above the ribbon cable connector is a socket for an optical cable. The laser needed for the 6.5 and 6.6 measurements is generated in the control unit and transmitted via the fibre optic cable into the detector unit and coupled out in the movable laser unit. The lemo connections are used for the trigger cable in the source measurement.

When measuring the current-voltage characteristic, a special feature must be observed at 0 V. The rotary knob must be turned from a higher voltage until it just indicates 0V. If it is turned further to the mechanical stop, a small bias voltage is applied to the sensor in the forward direction and it becomes conductive. This explains the red marked value in figure 3.3.

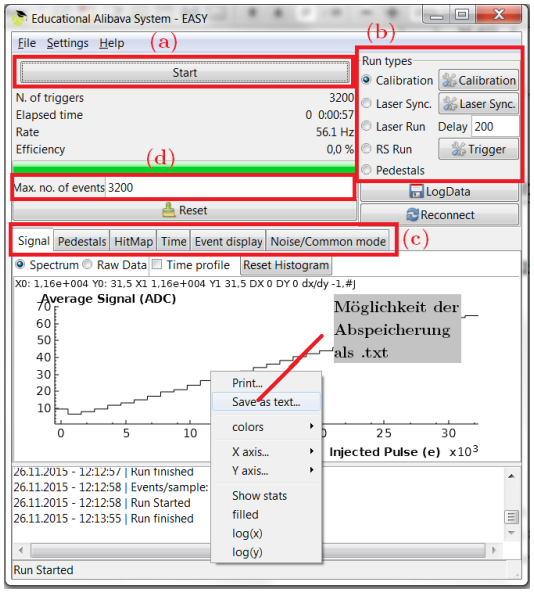

Fig. 5.7: Programme window of the Alibava-gui.

Figure 5.7 shows the Alibava-gui, which is used to control the Alibava system. With (a) the data recording can be started, area (b) determines the operating mode, with (c) the display of the data can be selected and with (d) the size of the statistics can be determined. By right-clicking on the graphs, the displayed measured values can be saved as .txt. It is possible to save the data in .h5 files by specifying a file via LogData before the measurement.

5.3 Experimental setup for source measurements

The detector unit is in a box lined with lead bricks on the sides and bottom. The lead serves as a shield for the radiation from the source used. Figure 5.8 shows the environment of the superstructure.

Before placing the source in the box in the designated place, the system must be correctly

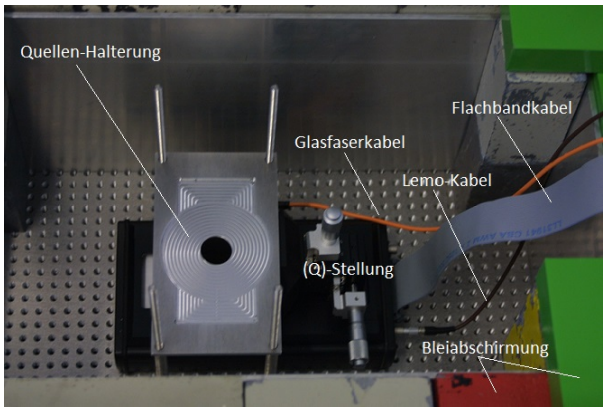

Fig. 5.8: Top view of the detector unit in (Q)-position with connected ribbon cable and Lemo cable in the lead shield.

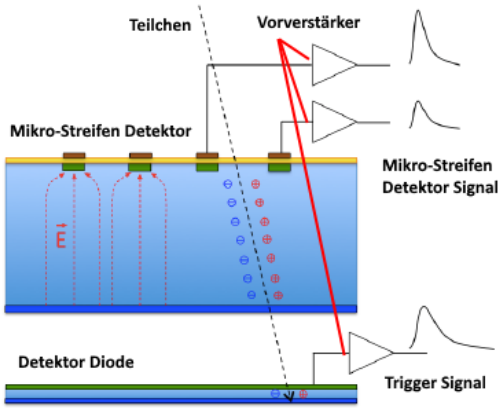

Fig. 5.9: Processed schematic representation of a cross-section through the sensor and the diode of the sensor installed in the EASy [Ali15].

wired. The procedure for the new wiring must be carried out in the same way as described in the first part of the trial instructions[14]. In addition, the LEMO cable must be plugged into the detector unit into the *Diode Trigger* connector and into the control unit into the *Trigger Pulse In* connector. The detector is to be operated in the Q position so that the carbon plate on which the source is positioned is directly above the sensor. Carbon fibre was chosen as the material because even at a very small thickness it is opaque, stable and thus permeable to ionising radiation such as electron [Ali15]. Only then should the source be positioned and the box closed. Since there is hardly any shielding upwards, handling above the box should be avoided.

5.4 Diode trigger

By detecting the electron-hole pairs generated when an ionising particle passes through, the sensor can determine the energy emitted. Figure 5.9 shows a schematic representation of how a signal is generated in the sensor, with each of the 128 strips connected to the *BEETLE chips* [Ali15].
An additional silicon diode is important for the source measurements. It is positioned several millimetres below the strip sensor and is supplied by a module-internal voltage source that cannot be controlled externally. It only detects electrons that have flown through the entire sensor and still have sufficient energy to create electron-hole pairs in the diode as well. If this diode registers a particle passage, a trigger signal is triggered, whereupon the control unit switches off the BEETLE chip.

[14]Page 13

5.5 Pedestals and noise

The sensor itself and the readout electronics, which will be discussed further in section 5, generate noise signals that interfere with the actual relevant signals. These signals are called noise. It is not possible to eliminate noise completely, but it is possible to reduce it to a minimum [Fra03].
he measured ADC(i,k) count that arises for a signal k at a strip i is shown in equation 12.

$$\mathrm{ADC}(i,k) = \mathrm{P}(i,k) + \mathrm{D}(k) + \mathrm{Signal}(i,k) \tag{12}$$

The mean value of the ADC counts for a strip without external signal(i,k) is called *pedestal* P(i) and is calculated from N measurements without signal source as follows:

$$\mathrm{P}(i) = \frac{1}{\mathrm{N}} \sum_{k=1}^{N} ADC(i,k). \tag{13}$$

Each of the 128 channels has a pedestal offset of about 500 ADC counts. The *Common Mode Shift* D(k) describes a global disturbance affecting all strips during an event. It is determined as follows:

$$\mathrm{D}(k) = \frac{1}{128} \sum_{i=1}^{128} (\mathrm{ADC}(i,k) - \mathrm{P}(i)). \tag{14}$$

The common mode shift across all stripes is also referred to as *Common Noise* [Ali15] and is i. A. Gaussian distributed around 0 [Fra03].
The noise of each strip is determined by taking the RMS[15] of the ADC counts after subtracting the pedestal and common mode shifts:

$$\mathrm{Noise}(i) = \sqrt{\frac{1}{\mathrm{N}-1} \sum_{k=1}^{\mathrm{N}} (\mathrm{ADC}(i,k) - \mathrm{P}(i) - \mathrm{D}(k))^2}. \tag{15}$$

For measurements where a true signal is expected, a second run of these calculations must be performed, where signals several standard deviations above the noise level are sorted out.

5.6 Analysis system

During signal generation of the strip sensors, the noise of the strips and the readout electronics is always converted into ADC counts and stored. A signal-to-noise cut is used to distinguish the relevant signal from the noise. This is done by dividing the signal

[15] Root-Mean-Square

generated by the β^- particle passing through by the noise of the strip. This is compared with the set $S/N_{textcut}$(in this experiment: 5). If the signal is larger, it is considered further in the analysis.
Various effects can cause clusters to form, which means that several neighbouring strips see one signal. Charge sharing occurs when particles pass near the edge of a strip. Here, the deposited charge goes to two different, neighbouring strips. In the effect of crosstalk, a signal in the readout chain of one strip induces a signal in the neighbouring strip. Particle paths that are not perpendicular to the surface can also run through several strips.

6 Measuring tasks

Help for carrying out the measurement tasks is given in section 7.

6.1 Preliminary tasks

a) Familiarise yourself with the reading of a micrometer screw. As an example, read off how many µm or mm the micrometer screw shows in figure 5.5 on page 13.
b) The sensor is examined with a ^{90}Sr source. How does the decay of yttrium-90 in the subsequent process affect the measurement of the energy spectrum?

6.2 Measurement of a current-voltage characteristic

Measure a current-voltage characteristic in 10 V steps and confirm the depletion voltage stated by the manufacturer from section 5.1. For the following measurements, unless otherwise requested, apply a voltage to the sensor at least 20 V higher than the depletion voltage determined. Justify this.

6.3 Pedestals and noise

Perform a *Pedestal Run* for 1,000 events.
a) Plot an overview of the pedestals and noise for each strip.
b) Graphically represent the values of the Common Mode in a meaningful way.

6.4 Calibration measurements

For this measurement task, it is sufficient to save the data as .txt by right-clicking on the graph.
a) Determine the optimum delay with a *Delay measurement* in the *Calibration Run* and enter the value in the Calibration window.
b) Record a calibration curve for five channels with the bias voltage above the depletion voltage. For one channel, additionally record a curve at a bias voltage of 0 V. (*Num. Pulses* = 256, *Charge (e-)* = 260 000).
   a) Plot the measured values of the *Calibration Runs* and their mean values.
   b) Determine the dependence of the injected charge on the measured ADC values with a 4th degree polynomial.
   c) Compare the curve at 0 V and above the depletion voltage.

6.5 Measuring the strip sensors by using the laser

a) Measure the optimal delay between laser signal and chip readout using the option *Laser Sync.*.
b) Investigate the structure of the strip sensor by recording 1,000 events for 35 points at 10 µm intervals.
c) Plot the signal of relevant strips as a function of the laser position. Determine from this the *pitch* of the strips, the extension of the laser on it and note the strip numbers.

6.6 Determination of the Charge Collection Efficiency

Using a laser

Increase the voltage from 0 to 200 V in 10 V steps and record a data set of 1,000 events for each step.

a) Investigate the efficiency of the detector as a function of the applied voltage by measuring one of the maxima from task 6.5 at different bias voltages with the laser in focus. Compare the beginning of the plateau with the depletion voltage determined in task part 6.2.
b) Determine the penetration depth a of the laser via a fit with equation (11).

Using a β^--source

Increase the voltage from 0 to 200 V in 10 V steps and record a data set of 10,000 events for each step.

a) Plot the mean cluster energy as a function of the applied voltage.
b) Compare the results between the CCE measurement with a laser and the source. Why do they differ?

6.7 Large source scan

Perform a *RS Run* for 1,000,000 events.

a) Represent the clusters per event and the channels per cluster in a meaningful way.
b) Display the number of events per channel (hitmap).
c) Plot the energy spectrum in ADC values and in keV.
d) Determine the mean value of the deposited energy and the MPV.
e) Interpret the mean value and evaluate the result.

7 Help for carrying out the measuring tasks

Evaluation script

To enable the choice of any evaluation software, an evaluation script is available that converts the measurement data into *.txt* files and performs some analysis steps. A folder containing this script is provided. The measurement data must be placed in suitable subfolders so that it is possible to run the script. Once the experiment is complete, the python script *execute.py* must be run. It should be noted that this takes a few minutes.

Measurement of a current-voltage characteristic

The measurement of the current-voltage characteristic is only controlled via the control unit. Nevertheless, this must be initialised with the computer. To do this, the system must be connected to the computer and the Alibava-gui must be started. If the system is initialised correctly, the red LED goes out and only the green LED lights up continuously. If this is not the case, the reset button on the back of the control unit must be pressed and the software restarted.
When measuring, proceed in such a way that the desired bias voltage is first set via the rotary knob. Note that the bias voltage of 0 V must be set carefully from a higher voltage, as turning the knob further will apply a low voltage in the forward direction, causing the sensor to conduct.
Wait a few seconds before recording the leakage current and note the value.
After measuring from 0 to 199 V, plot the leakage current as a function of the applied bias voltage and estimate the depletion voltage from the graph.

Evaluation of pedestals and noise

A *Pedestal Run* shall be performed by saving a file under *Pedestal/Pedestals.h5* via *Log-Data* and starting a *Pedestal Run* **then**. The evaluation script produces a text file named *pedestals.txt* which contains measured signals of all channels for each element. The evaluation is to be carried out using the definitions in chapter 5.5.

Calibration measurements

During the calibration measurement, the control unit sends a defined electron pulse to the BEETLE via the ribbon cable. This is necessary to be able to convert the ADC counts into charge in the further course of the experimental tasks. The BEETLE then transmits the measured ADC counts to the control unit. If these are plotted as a function of the transmitted electron pulse, the calibration curve for the charge is obtained.

To do this, select the option *Calibration Run* in the programme window via area (b) (cf. figure 5.7). Further parameters can be set via a second programme window, which can be opened by pressing *Calibration*. The window can be seen in figure 7.1. First, a *Delay* scan must be carried out. This optimises the interval between the signal and the readout of the BEETLE. The maximum of the resulting curve is to be entered under *Delay* in the *DAQ general* window. This is under the tab *Settings* the menu item *DAQ*. Typically, the delay has a value around 65 ns. In the same menu, the channel to be examined can be selected, as shown in figure 7.2.

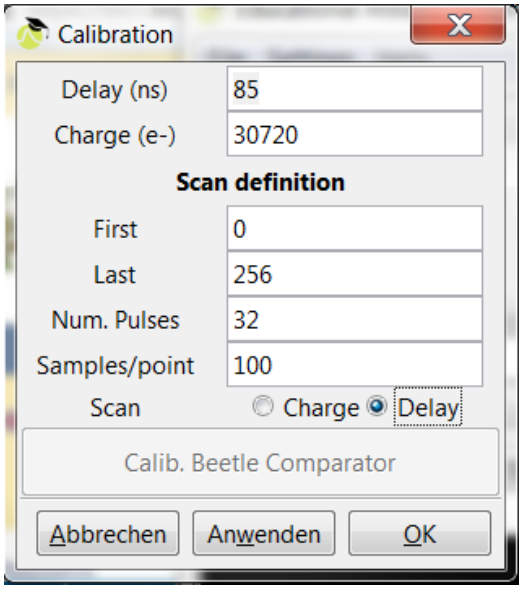

Fig. 7.1: Parameters of the Calibration Run.

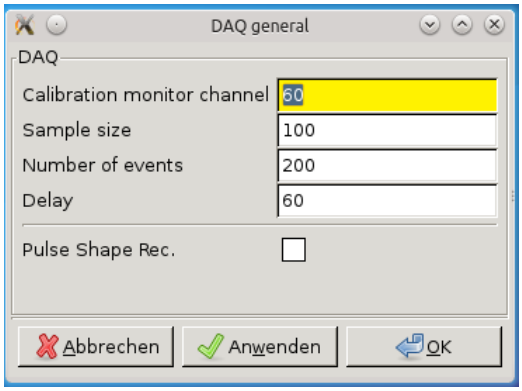

Fig. 7.2: *DAQ general* menu overview.

The *Samples/point* option in the *Calibration* menu defines how many measurements are taken per data point and the *Num.Pulses* the number of pulses that are examined.

The data is taken directly from the graph and saved in a text file (in the folder *Calib*) with a right click. When determining the polynomial, restrict the fit range so that a sensible fit is possible.

Measuring the strip sensors by using a laser

The strip structure on the semiconductor sensor can be detected by using the laser, because it is reflected at the metallisation in the middle of the strips. Therefore, it cannot penetrate into the semiconductor there and no signal can be generated. By measuring a few periods, the distance between the strip sensors can be determined from the interval between the minima.

Fig. 7.3: Fibre optic cable to connect the laser.

First, the laser must be synchronised with the system. To do this, select the operating mode *Lasersync.* in section (b) of the programme window and start data acquisition. The graphic interface shows the measured ADC counts under the tab *Signal* in relation to the delay between laser and readout. From the maximum, the optimal delay is to be entered into the form field next to *Laser Run*. The measurement data can be saved and plotted by right-clicking. If there is no peak, it is most likely because the laser is exactly above a metallisation. In this case, the horizontal micrometer screw can be used to move the laser over the sensor. Another possibility is to strongly defocus the laser, as this will hit a larger area of the sensor.

If the laser is synchronised, select the *Laser Run* via area (b) of the programme window. Under the tab *Event Display* the measured signal of the individual strips can be displayed. By turning the horizontal micrometer screw a maximum is to be searched for. Then the vertical micrometer screw is used to move the laser up and down until it is focused and thus has the smallest possible diameter on the sensor. This can be recognised by the fact that the peak becomes maximum, because in this case the signal is only detected by one strip.

For evaluation, each measuring point must be saved as a separate *.h5* file in the Laserscan folder. Start the naming with *Laser_1.h5*, start a *Laser Run* and turn the horizontal micrometer screw 10 μm further on it. Save another *.h5* under the name *Laser_2.h5* and continue in this way until 35 measuring points are recorded.

The evaluation script performs a correction using the pedestal scan and then outputs a *.txt* file with a 35x128 matrix with the mean signal for each channel in each positioning. The position-dependent signals of the relevant channels are now to be displayed in a plot so that all points are shown for all channels with a definite signal.

Determination of the Charge Collection Efficiency (Laser)

The procedure here is similar to that in measurement task 6.5. The horizontal and vertical position of the laser is fixed, while the applied bias voltage is varied.

The laser is to be focused as in task 6.5, and a maximum is to be searched for. A new series of measurements must then be started by creating a *LogData* file in the *CCEL* folder via *.h5*. The file name must contain the applied voltage and no other numbers.

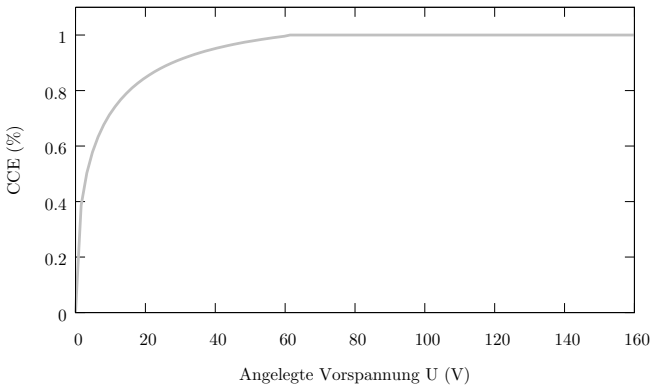

Fig. 7.4: Theory curve of the efficiency of the detector as a function of the applied bias voltage. The plateau starts at $U_{dep} = 60\,\mathrm{V}$, as the sensor is fully depleting from this voltage.

The laser run must then be started. The script creates *.txt* files that contain the average value of each channel for each measurement.

To determine the penetration depth of the laser into the sensor, a fit over the mean penetration depth a from equation (11) is to be carried out via a plot program. Here, only the channel hit by the laser in the area below the depletion voltage is to be considered. If necessary, additional fit parameters, e.g. for scaling, can be inserted. Figure 7.4 shows the theory curve of the Charge Collection Efficiency.

Determination of the Charge Collection Efficiency (Source)

To determine the charge collection efficiency for a source measurement, a similar procedure is to be followed. A source scan with 10,000 events is to be carried out at different voltages. The data is saved as in the previous part of the task, but here in the folder *CCEQ*. With the help of the evaluation script, the clusters are determined from the raw data. Add up the entries of a cluster and use the mean value of the counts in a cluster as a comparison value. For correct timing, the menu item *Latency* must be selected in the tab *Settings* and set to 129. Enter the number of events for the data recording in the *Event* field.

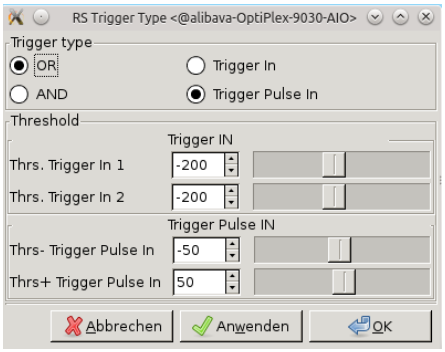

Fig. 7.5: *Trigger* menu for the *RS Run*.

Open the *Trigger* menu from the main menu and set the values as shown in figure 7.5. A measurement is started with the selection *RS Run*.

Various *.txt* files are created. In the file *Cluster_adc_entries.txt*, each line contains a single

cluster with all ADC entries assigned to the cluster.

Large source scan

The file shall be saved under the name *RS_Run.h5* with *LOGData* in the folder *RSScan*. Then start the *RS Run*.
The evaluation script evaluates the data with a signal-to-noise cut and determines the *pedestals*, the *noise*, the *common mode* and generates clusters. The file outputs four .txt files named according to their contents.
For further analysis, the conversion of the ADC charge spectrum into a keV spectrum is to be performed using the fit from task 6.7. To do this, convert the individual ADC-count entries into energies and then add up all the energies of a cluster.

Bibliography

[Ali15] Alibavasystems (Hrsg.): *Activity Book for Students*. First Edition. Barcelona: Alibavasystems, 2015

[Bet96] Bethge, Prof. Dr. K.: *Kernphysik*. Springer-Verlag Berlin Heidelberg, 1996

[CER16] CERN: *Internetpräsenz CERN*. `http://home.cern/about/experiments`. Version: Jan 2016

[Fra03] Fraden, Jacob: *HANDBOOK OF MODERN SENSORS*. Third Edition. San Diego : Springer Science + Business Media, LLC, 2003

[Har09] Hartmann, F.: *Evolution of Silicon Sensor Technology in Particle Physics*. Berlin : Springer, 2009

[Kit02] Kittel, C.: *Einführung in die Festkörperphysik*. 13. Auflage. München : Oldenbourg Verlag, 2002

[Kuc11] Kuchling, H.: *Taschenbuch der Physik*. München : Carl-Hanser Verlag, 2011

[Leo87] Leo, Dr. William R.: *Techniques for Nuclear and Particle Physics Experiments*. 2. Auflage. Springer-Verlag Berlin Heidelberg, 1987

[Lid96] Lide, D.: *CRC Handbook of Chemistry and Physics*. 77th Edition. Boca Raton : CRC Press, 1996

[Peq08] Pequenao, Joao: *Computer generated image of the whole ATLAS detector*. `http://cds.cern.ch/record/1095924`. `http://cds.cern.ch/record/1095924`. Version: Mar 2008

[PS13] Pequenao, Joao ; Schaffner, Paul: *An computer generated image representing how ATLAS detects particles*. `https://cds.cern.ch/record/1505342`. `https://cds.cern.ch/record/1505342`. Version: Jan 2013

[Rau] Rausch, Rene: *Periodensystem-online*. `http://www.periodensystem-online.de/index.php`

[Sch14] Schorlemmer, Dr. A.: *Monitoring Radiation Damage in the ATLAS Pixel Detector*. Göttingen, Georg-August Univesität Göttingen, Diss., 2014

[SL13] Sze, S. ; Lee, M.-K.: *Semiconductor devices : physics and technology*. 3rd ed. Wiley & Sons Singapore Pte. Ltd, 2013